Amplification-free electrochemical biosensor detection of circulating microRNA to identify drug-induced liver injury

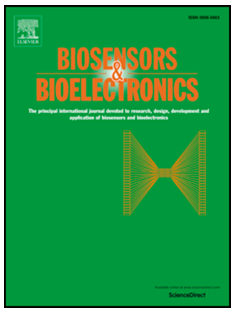

Amplification-free electrochemical biosensor detection of circulating microRNA to identify drug-induced liver injury

Appan Roychoudhury, James W. Dear, Maïwenn Kersaudy-Kerhoas, Till T. Bachmann

PII: S0956-5663(23)00240-3

DOI: https://doi.org/10.1016/j.bios.2023.115298

Reference: BIOS 115298

To appear in: *Biosensors and Bioelectronics*

Received Date: 5 December 2022

Revised Date: 23 March 2023

Accepted Date: 4 April 2023

Please cite this article as: Roychoudhury, A., Dear, J.W., Kersaudy-Kerhoas, Maï., Bachmann, T.T., Amplification-free electrochemical biosensor detection of circulating microRNA to identify drug-induced liver injury, *Biosensors and Bioelectronics* (2023), doi: https://doi.org/10.1016/j.bios.2023.115298.

CRediT authorship contribution statement

Appan Roychoudhury: Conceptualization, Methodology, Data curation, Formal analysis, Investigation, Validation, Writing - original draft. **James W. Dear:** Investigation, Validation, Resources, Writing - review & editing, Funding acquisition. **Maïwenn Kersaudy-Kerhoas:** Writing - review & editing, Funding acquisition. **Till T. Bachmann:** Conceptualization, Methodology, Investigation, Validation, Resources, Writing - review & editing, Funding acquisition.

Amplification-free electrochemical biosensor detection of circulating microRNA to identify drug-induced liver injury

Appan Roychoudhury[1], James W. Dear[2], Maïwenn Kersaudy-Kerhoas[1,3], Till T. Bachmann[1*]

[1] *Infection Medicine, Edinburgh Medical School: Biomedical Sciences, University of Edinburgh, Chancellor's Building, 49 Little France Crescent, Edinburgh EH16 4SB, UK*

[2] *Centre for Cardiovascular Science, University of Edinburgh, The Queen's Medical Research Institute, 47 Little France Crescent, Edinburgh EH16 4TJ, UK*

[3] *Institute of Biological Chemistry, Biophysics and Bioengineering, Heriot-Watt University, Edinburgh EH14 4AS, UK*

*Corresponding author: Phone: +44 (0) 131 242 9438; E-mail: till.bachmann@ed.ac.uk

Abstract

Drug-induced liver injury (DILI) is a major challenge in clinical medicine and drug development. There is a need for rapid diagnostic tests, ideally at point-of-care. MicroRNA 122 (miR-122) is an early biomarker for DILI which is reported to increase in the blood before standard-of-care markers such as alanine aminotransferase activity. We developed an electrochemical biosensor for diagnosis of DILI by detecting miR-122 from clinical samples. We used electrochemical impedance spectroscopy (EIS) for direct, amplification free detection of miR-122 with screen-printed electrodes functionalised with sequence specific peptide nucleic acid (PNA) probes. We studied the probe functionalisation using atomic force microscopy and performed elemental and electrochemical characterisations. To enhance the assay performance and minimise sample volume requirements, we designed and characterised a closed-loop microfluidic system. We presented the EIS assay's specificity for wild-type miR-122 over non-complementary and single nucleotide mismatch targets. We successfully demonstrated a detection limit of 50 pM for miR-122. Assay performance could be extended to real samples; it displayed high selectivity for liver (miR-122 high) comparing to kidney (miR-122 low) derived samples extracted from murine tissue. Finally, we successfully performed an evaluation with 26 clinical samples. Using EIS, DILI patients were distinguished from healthy controls with a ROC-AUC of 0.77, a comparable performance to qPCR detection of miR-122 (ROC-AUC: 0.83). In conclusion, direct, amplification free detection of miR-122 using EIS was achievable at clinically relevant concentrations and in clinical samples. Future work will focus on realising a full sample-to-answer system which can be deployed for point-of-care testing.

Keywords: Drug-induced liver injury; microRNA detection; electrochemical impedance spectroscopy; continuous-flow measurements; point-of-care diagnostics

1. Introduction

Drug-induced liver injury (DILI) is a common adverse effect of many drugs, poses a serious health risk, and has a significant impact on healthcare expenditures (Giacomini et al. 2007; Wang et al. 2009). DILI is responsible for nearly 50% of acute liver failure in Europe and the United States (Bernal and Williams 2018; Kaplowitz 2005; Lee 2013). Paracetamol (acetaminophen) overdose is the most frequent cause of DILI in the Western world (Dear et al. 2018). In the United Kingdom, paracetamol overdose results in a substantial number of hospital visits (~100,000), hospital bed occupancy (~60,000 beds) and NHS cost (~£50 million) every year (Park et al. 2015). In the United States, paracetamol overdose is responsible for ~82,000 hospital visits and ~450 deaths annually (Lee 2004). In addition to paracetamol, the National Institutes of Health (NIH) LiverTox database (livertox.nih.gov) has identified more than 1140 drugs which can cause serious liver injury. Non-paracetamol 'idiosyncratic' DILI has an annual incidence of about 14-19 per 100,000 inhabitants (Björnsson et al. 2013; Sgro et al. 2002). In a multi-national European prospective DILI registry, antibacterials were the most commonly implicated medicines (Björnsson et al. 2022). In China, the annual incidence of DILI is estimated to be 23.8 per 100,000 persons (Shen et al. 2019).

DILI is one of the key challenges for the drug development. It can lead to early market removal of new drugs after launch, resulting huge financial losses for the pharmaceutical companies. A problem in this context is the lack of reliable diagnostic and prognostic biomarkers, making it difficult to identify patients who are at risk. MicroRNA122 (miR-122) is significantly raised in the circulation of DILI patients, and can be detected earlier than conventional clinical liver biomarkers e.g., alanine aminotransferase (ALT) and aspartate aminotransferase (AST) (Starkey Lewis et al. 2011; Starkey Lewis et al. 2012). ALT and AST activity increases 12-16 hours after paracetamol overdose, whereas miR-122 can diagnose liver injury within 4 hours (Vliegenthart et al. 2015b). While ALT is the gold standard biomarker

for hepatocyte injury, it lacks tissue specificity, and can cause false positives, reducing the confidence in DILI diagnosis (Starkey Lewis et al. 2011). In contrast, miR-122 is distinctly and abundantly expressed in the liver, representing 70% of the total hepatocyte miRNA hepatic complement (~40,000 copies per hepatocyte) (de Rie et al. 2017). During liver injury, miR-122 is released from necrotic hepatocytes, causing high miR-122 concentrations in the circulation (Wang et al. 2009). After paracetamol overdose and liver injury, the miR-122 concentration can rise up to 100 to 10,000 fold higher than the healthy concentration (Antoine et al. 2013; Dear et al. 2014; Starkey Lewis et al. 2011). In vitro, miR-122 has been demonstrated as a biomarker of cellular toxicity during the development of new drugs (Kia et al. 2014). The US Food and Drug Administration (FDA) has provided formal regulatory support for the miR-122 to be utilised as an exploratory DILI biomarker in the clinical trials.

Presently, different analytical techniques such as northern blot (Válóczi et al. 2004), real-time quantitative polymerase chain reaction (qRT-PCR) (Lundegard et al. 2015; Yu et al. 2013), microarray (Wang and Xi 2013) and next-generation sequencing (Rahmann et al. 2013) are used for microRNA detection and quantification. PCR-based methods have been widely used as gold standard due to their high sensitivity and low detection limit. However, the requirement for a thermal cycler and the use of multiple enzymes, particularly in reverse transcription PCR-based methods, leads to complex workflow and higher measurement cost. RNA instability during the measurements, the need for well-trained operators, operator variability and high instrumental and energy requirement limit the application of PCR particularly in clinical practice. Most importantly, PCR and other conventional techniques are not suitable for point-of-care setup. Several attempts were made for point-of-care testing (POCT) of microRNA using portable readers, like lateral flow strips (Wang et al. 2022; Zhou et al. 2020), personal glucose meter (Gong et al. 2021; Huang et al. 2020), pressure meter (Shi et al. 2018) and mobile phone (Kerr et al. 2021), and by combining CRISPR-Cas, duplex-

specific nuclease, substrate-linked magnetic beads and electrochemiluminescence molecular beacon systems. However, there are still limitations with miRNA POCT, such as the long-term storage stability of expensive enzymes and antibodies, and the need for an additional magnetic separation method or instruments for signal detection (Wang et al. 2023). Furthermore, the detection without target amplification at POCT setup is challenging due to the lower sample volume availability and often very low expression levels of miRNA. Assays that can perform miRNA POCT rapidly and precisely and are easy to build and operate are still needed.

POCT compatible biosensors are promising alternatives to PCR and other traditional methods because of their low complexity, low cost, ease of operation, and scalability for mass production (Liu et al. 2020; Wang 2006). In this direction, Shin Low et al. designed a disposable biosensor for miR-21 detection based on reduced graphene oxide/gold composite modified screen-printed electrode, a circuit board, and a Bluetooth-enabled smartphone reader equipped with specially designed Android application (Shin Low et al. 2020). Bruch et al. used microfluidic biosensor with CRISPR/Cas13a system for simultaneous detection of miR-19a and miR-20b from a single specimen by combining the single-channel design with a microfluidic stop-flow protocol (Bruch et al. 2021). Likewise, if miR-122 could be measured by an easy-to-use point-of-care biosensor, this would constitute a step forward in terms of improving patient safety. For instance, patients may have their liver health monitored at home, with findings being communicated electronically to their doctor nearly instantly. This would allow for the early detection of signs of hepatotoxicity and the cessation of drug treatment before more severe liver damage develops. Such a test would enable drug developers to increase liver safety monitoring schedules without the need for patients to go to the study site, which frequently presents a considerable logistical issue in clinical trials. Significant gains in patient safety might result from this, as well as the ability to identify liver safety hazards sooner

in drug development programmes and perhaps make it easier to register medications that address unmet medical requirements.

Among various bio-sensing techniques, electrochemical-based detection has attracted interest owing to its robustness, low complexity, cost-effectiveness and miniaturisation capability (Ronkainen et al. 2010; Roychoudhury et al. 2017; Turner 2013). Electrochemical biosensors are often useful in point-of-care setup due to simple operation and ease in miniaturisation (Roychoudhury et al. 2016; Wang 2006). We have previously demonstrated the use of electrochemical impedance spectroscopy (EIS), which is particularly well-suited for developing rapid and sensitive assays for nucleic acid hybridisation-based detection without the need of labelling of targets (Kersaudy-Kerhoas et al. 2022; Roychoudhury et al. 2022). EIS allows for detailed evaluation of interfacial property changes at the electrode surface caused by the probe modification and subsequent target hybridisation (Lisdat and Schäfer 2008). The EIS readout enables for fast and sensitive detection with minimal steps using handheld instrumentations, providing high utility in wider use and point-of-care applications (Lu et al. 2015; Yang and Chen 2017).

Biosensors often rely on diffusion of targets from the bulk solution to the surface-immobilised probes. This purely diffusion-controlled binding results in lengthy procedures with slow binding kinetics and reduced binding efficiency (Liu et al. 2003; Tavallaie et al. 2018). However, POCT requires shorter time to results which could be achieved by faster transport of target molecules to their binders on the sensor surface. Several attempts have been made to improve hybridisation kinetics by facilitating mass transfer, such as by using direct electric field (Edman et al. 1997; Sosnowski et al. 1997), magnetic actuation (Tavallaie et al. 2018), acoustic micromixer (Liu et al. 2003) and pumping of target solution (Kim et al. 2006; Wang et al. 2011). In the present work, we used a microfluidic system with a continuous flow of target solution for enhanced transport of miR-122 targets to immobilised PNA probes. We

optimised the hybridisation temperature in flow conditions to enhance target specificity and verified the specificity performances against non-complementary, nearly-complementary, common isoforms and single nucleotide mismatch targets. After confirmation of selectivity using murine tissue samples, we distinguished liver injured human serum samples from the healthy controls with a comparable performance to qPCR.

2. Experimental

2.1. Reagents, probes and targets

Tris(2-carboxyethyl)phosphine hydrochloride (TCEP), dimethyl sulfoxide (DMSO), dimethylformamide (DMF), sulfuric acid (H_2SO_4), monosodium phosphate (NaH_2PO_4), disodium phosphate (Na_2HPO_4), sodium chloride (NaCl), potassium ferricyanide [$K_3Fe(CN)_6$] and potassium ferrocyanide [$K_4Fe(CN)_6$] were purchased from Sigma-Aldrich (Gillingham, UK). 6-Mercapto-1-hexanol (MCH) and 1,6-hexanedithiol (HDT) were procured from ProChimia Surfaces (Gdynia, Poland). All of the other chemicals were of analytical grade unless otherwise stated. All of the aqueous solutions were made with deionised water (resistivity > 18 MΩ cm) from a Millipore MilliQ water purification system (Bedford, MA, USA). The specific and non-specific peptide nucleic acid (PNA) single-stranded probes for miR-122 target sequence were ordered via Cambridge Research Biochemicals (Cleveland, UK) and obtained from Panagene (Daejeon, South Korea). Probes (> 95% HPLC purified) were synthesized with a linker consisting of three ethylene glycol units (abbreviated as AEEEA) and a terminal thiol group on either N-end (equivalent to 5'-end of DNA) or C-end (equivalent to 3'-end of DNA) of the PNA for self-assembled monolayer (SAM) formation on gold electrode surface. The PNA stock solutions were prepared in 50% (v/v) dimethylformamide (DMF) aqueous solution and kept at -20°C during storage. The complementary and nearly or non-complementary RNA target sequences were obtained from Metabion (Martinsried, Germany).

Stock solutions of the RNA targets were prepared in nuclease-free deionised (DI) water and stored at -80°C. The sequence and structural details of PNA probes and RNA targets are provided in **Table S1** of the **Supporting Information**.

2.2. Electrode preparation

Screen-printed gold electrodes (DRP-C223BT, DropSens) were functionalised with PNA probes according to the protocol used in our earlier study (Roychoudhury et al. 2022). Briefly, after being electrochemically cleaned (cyclic voltammetry, 0 - 1.6 V potential range, 100 mV/s scan rate and 10 cycles), the gold working electrode was modified with a ternary MCH/HDT/PNA probe layer, by preparing 1.5 µM PNA probe solution with 100 µM MCH and 200 µM HDT as spacers and 5 mM TCEP as reducing reagent. 4.5 µL of this mixed probe solution was placed on the working electrode and kept in a humid chamber for 16 h to immobilise the probes, followed by 2 h of blocking with 1 mM MCH solution to avoid non-specific adsorptions. Finally, the probe-functionalised electrodes were rinsed with 50% (v/v) DMSO aqueous solution and then DI water before being employed for further impedance measurements. Details on different electrode characterisation techniques, as well as the collection and preparation of clinical samples are presented in **Supporting Information**.

2.3. Electrochemical impedance spectroscopy (EIS) measurements

EIS measurements were conducted in a frequency range of 0.3 Hz to 100 kHz with an AC signal of 10 mV rms amplitude at the measured open circuit potential using an EIS measurement buffer (10 mM sodium phosphate, pH 7, 20 mM sodium chloride and 0.2 mM potassium ferri/ferrocyanide redox mediator). EIS studies were performed both in no-flow and flow conditions, with a peristaltic pump controlling the flow rates. During the measurements, the functionalised electrodes were placed inside a flow cell which was fitted with a closed-loop continuous flow system. As shown in **Scheme 1**, the closed-loop assembly was prepared after

connecting the sample reservoir with the flow cell back and forth via the multichannel dispenser peristaltic pump (ISMATEC, ISM930C) and silicone tubings (0.79 mm internal diameter). The complete volume of the closed-loop system was 600 µL. Within that system, the flow cell volume was 80 µL. The flow cells were built with an aluminium base and a poly(methyl methacrylate) (PMMA) top layer to perform EIS measurements in a closed environment and at varied elevated temperatures without sample evaporation. The temperature was regulated using the hotplate when the flow cell was placed over the hotplate surface. To prevent the leakage during flow studies, the measurement chamber was encircled by a rubber O-ring, and the top PMMA and bottom metal parts of the flow cell were fastened using two screws on two opposite sides of the cell. The temperature of the samples to be added in the measurement chamber was maintained by placing the sample reservoir in a heat block system (Starlab, N2400-4002). The flow cells were connected with the potentiostat through a multiplexing module in order to serially record the multiple measurements in the same run. The potentiostat operation was controlled by Nova 2.1 software and the charge transfer resistance (Rct) values were collected from the equivalent Randles' circuit after fitting the data from the recorded Nyquist plots in a faradaic EIS measurement. During the design of the Randles' equivalent circuit, a constant phase element (as non-ideal capacitance) was employed instead of the double layer capacitance (Cdl) in parallel with Rct and the Warburg element. The EIS measurements were taken pre and post hybridisation with a 60 min sample incubation using the probe-functionalised electrodes and the increase in Rct value by dividing pre (baseline measurement) to post (sample measurement) hybridisation was mentioned as the 'Fold change' and used to plot the EIS data (see **Scheme 1**). All the EIS studies were performed in triplicates under identical conditions unless otherwise stated.

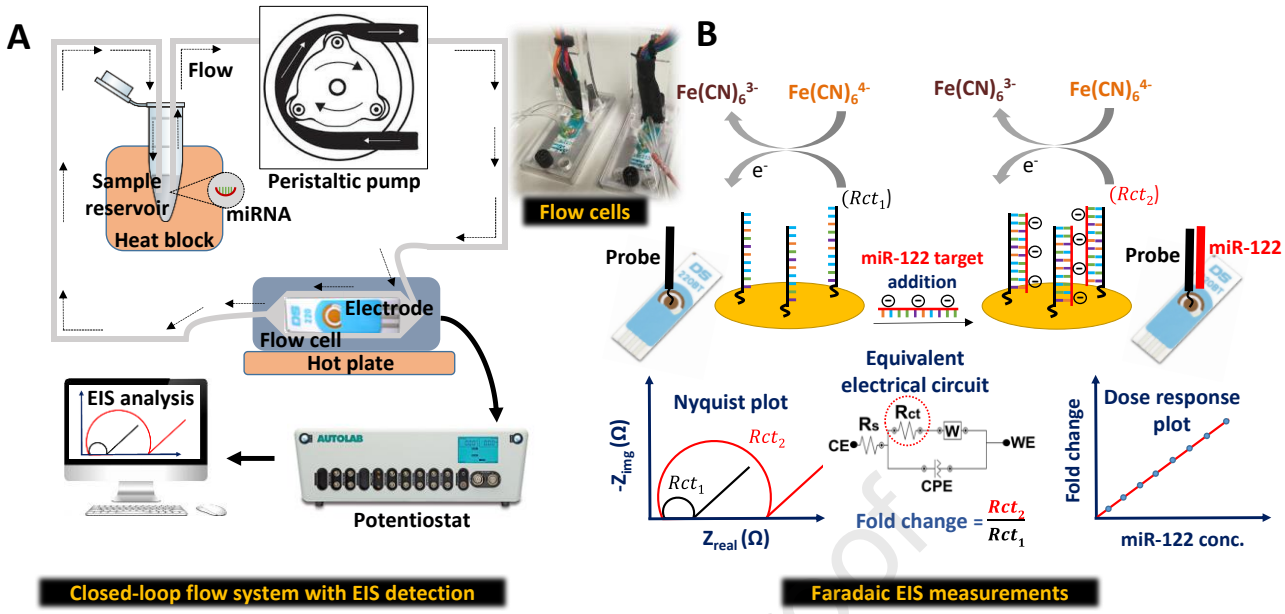

Scheme 1 - Closed-loop flow system for direct detection of miRNA using electrochemical impedance spectroscopy (EIS). (A) Schematic demonstrating an integrated electrochemical and closed-loop continuous flow system. Inset shows picture of flow cells used in present study; (B) illustration showing our faradaic EIS measurements for miR-122 sensing and our interpretation on recorded EIS spectra. We used complementary probe sequence and negatively charged ferri/ferrocyanide redox couple [$Fe(CN)_6^{3-/4-}$] for sequence specific detection of miR-122. Following hybridisation of miR-122 with the probe, there is an increase in negative charge on the electrode surface, which causes an increase in charge transfer resistance (Rct) for the redox couple in a faradaic EIS measurement. Equivalent electrical circuit was used to interpret the EIS Nyquist plots, and the Rct enhancement is proportional to the miR-122 hybridisation. CE, WE, Rs, W and CPE represent counter electrode, working electrode, solution resistance, Warburg element and constant phase element, respectively.

3. Results

3.1. Characterisation of electrode surface after probe functionalisation

The presence of PNA probes on the electrode surface following immobilisation was confirmed using atomic force microscopy (AFM), scanning electron microscopy (SEM), energy-dispersive X-ray spectroscopy (EDX) and cyclic voltammetry (CV). The AFM micrograph of the bare screen-printed gold working electrode (**Figure 1A**) taken in a 10 × 10

μm^2 scan area revealed a rough surface with porous morphology due to the presence of screen printed gold microparticles. The bare electrode showed a mean roughness (Ra) of 448.7 nm, a root mean square roughness (Rq) of 589.8 nm, and a roughness factor of 1.719. The electrode surface appeared less porous after probe immobilisation (**Figure 1B**), and the roughness parameters increased, with Ra = 460 nm, Rq = 613 nm and roughness factor 1.792. The line profiles obtained from AFM surface profile analysis (see **Figures S1**) demonstrate an increase in baseline height following the probe immobilisation, confirming less porous surface morphology of the electrode after modification with the probes. For further comparison, SEM, EDX and CV studies were conducted and the results are shown in **Figure 1C-1F**, and explained in **Supporting Information**.

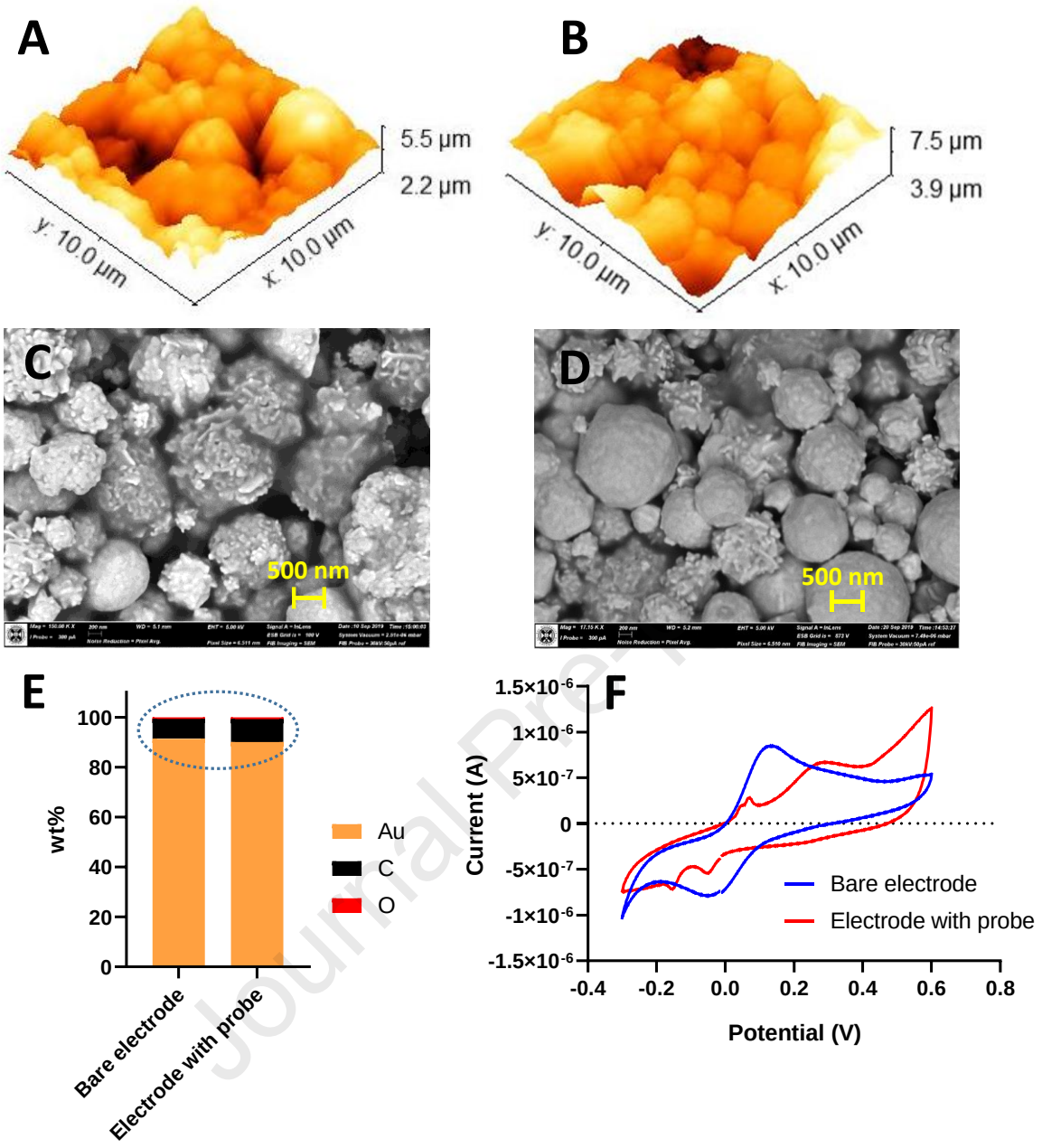

Figure 1 - Surface immobilisation of probes. Three-dimensional AFM micrographs of (A) bare electrode and (B) electrode after PNA probe functionalisation; SEM images (150,000 times magnification with 500 nm scale bar) of (C) bare electrode and (D) electrode after PNA probe functionalisation; (E) EDX spectra of bare electrode and probe-functionalised electrode; (F) cyclic voltammograms of bare electrode and probe-functionalised electrode in 10 mM sodium phosphate buffer, pH 7 with 20 mM sodium chloride and 0.2 mM potassium ferri/ferrocyanide redox mediator at a scan rate of 50 mV/s.

3.2. MiRNA detection in static and flow conditions

Probe-functionalised electrodes were tested for detection of miR-122 using hybridisation-based assay and EIS measurements in a closed-loop flow system. We analysed the hybridisation performance in no-flow and flow conditions to determine the hybridisation efficiency with faster mass transport under flow conditions. We found a > 3.5 fold rise in hybridisation signal from EIS measurements of miR-122 target in the flow conditions (100 µL/min onwards) as compared to no-flow (0 µL/min) (**Figures S2**). No further increase in hybridisation signal was observed above 100 µL/min flow rate (tested up to 900 µL/min).

3.3. Influence of flow rate and temperature on miRNA hybridisation signal

For more detailed evaluation of the effect of flow rate on hybridisation signal, the flow rate of the system was increased in 50 µL/min steps. The highest signal from miR-122 hybridisation was observed at 100 µL/min, afterwards signal remained almost constant in higher flow rates (**Figure 2A**). We determined the flow parameters at 100 µL/min to evaluate the fluid flow behaviour inside the flow cell and its influence on the hybridisation signal. For details, please see **Supporting Information**.

We optimised the hybridisation temperature at a fixed flow rate (100 µL/min) by varying the assay temperature (21 - 60°C). We observed an optimum of the hybridisation signal at 40°C (**Figure 2B**). At elevated temperatures, the buffer control signals became marginally higher than at room temperature. In summary, conditions of 100 µL/min flow rate and 40°C assay temperature were optimal and therefore used further in subsequent studies.

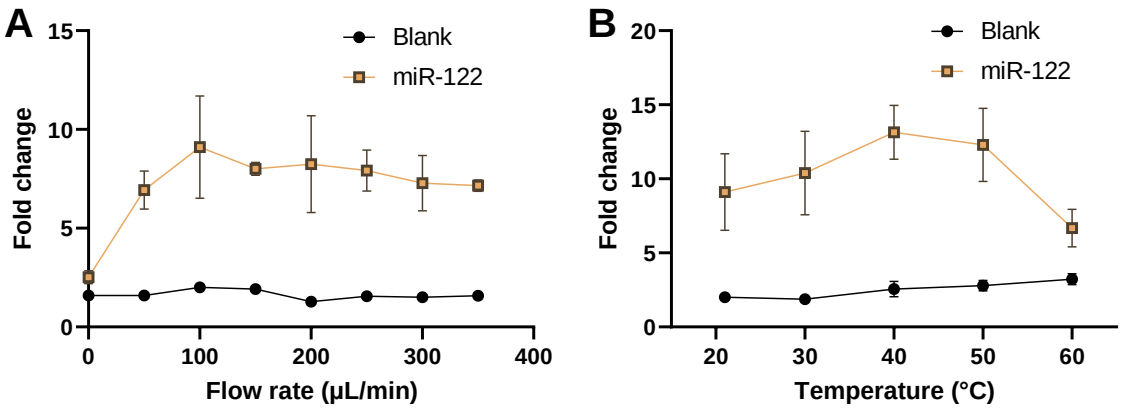

Figure 2 - Influence of flow rate and temperature on sensor response. (A) EIS signals (fold change increase from baseline to post hybridisation sample measurements) from electrodes functionalised with 1.5 µM P-miR-122 after 60 min incubation with buffer (blank) or 10 nM miR-122 at different flow rates (0 - 350 µL/min); (B) EIS signals (fold change) from electrodes functionalised with 1.5 µM P-miR-122 at 100 µL/min flow rate and at different hybridisation temperatures (21 - 60°C) after 60 min incubation with buffer (blank) or 10 nM miR-122. All data represent the mean ± SD; n = 3.

3.4. Dose dependent detection of miR-122

The closed-loop flow system was used to determine the sensitivity and detection limit for miR-122 detection at 100 µL/min and 40°C. The kinetics studies (**Figure 3A**) with varying target concentrations (0 - 50 nM) show an increase in EIS signals with increasing target concentrations. Furthermore, we found no saturation in hybridisation signals for our closed-loop flow system up to 5 nM target concentration, over a 60 minute sample incubation time. However, at concentrations of 10 nM and higher, distinct signal saturations were seen, with faster saturations at higher concentrations overall. We used the 60 min end-point reading to generate dose response curve (**Figure 3B**). The sensors produced a signal increase with rising concentrations of miR-122 with linear enhancement in between 1 and 50 nM miR-122. We calculated an assay sensitivity of 6.92×10^{-4} fold change/pM for miR-122 in the linear range

and a detection limit of 50 pM (equivalent to 30 fmole) based on the blank measurements (McNaught and Wilkinson 1997).

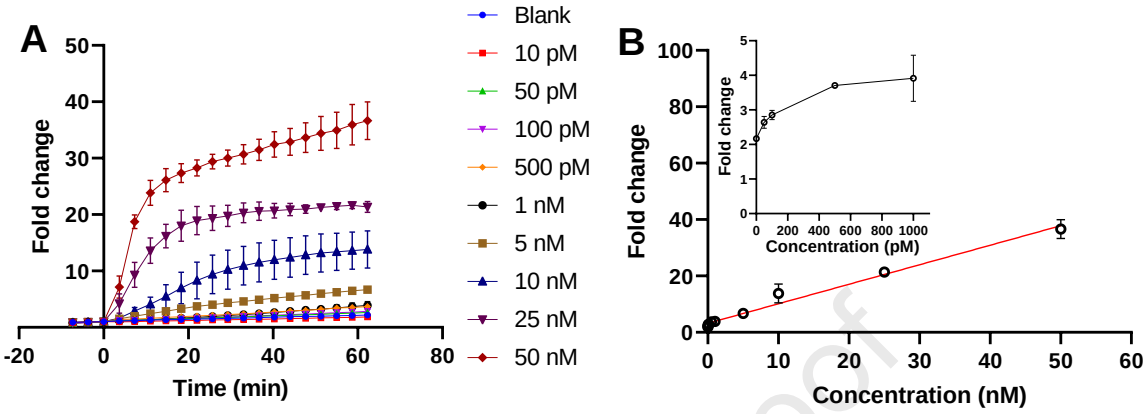

Figure 3 - miR-122 sensitivity studies in closed-loop flow format. (A) EIS signals (fold change) over time (Baseline: -8 - 0 min; miR-122 target addition; Hybridisation: 3 - 62 min) of 1.5 µM P-miR-122 functionalised electrodes with different concentrations (0 - 50 nM) of miR-122 target at 100 µL/min flow rate and 40°C hybridisation temperature; (B) 60 min end-point data after miR-122 target hybridisation at different concentrations (0 – 50 nM). The following equation has been calculated from the regression line: Fold change = 6.92×10^{-4} $(pM)^{-1} \times$ [miR-122] (pM) + 3.22 with $R^2 = 0.97$. Inset shows 60 min end-point miR-122 hybridisation data in 0 to 1000 pM concentration range. All data represent the mean ± SD; n = 3.

3.5. Specificity studies for miR-122 detection

We studied specificity of our biosensors, functionalised with the probe (P-miR-122) specific for the miR-122 target in flow condition (100 µL/min) by comparing it to a non-specific (control) probe (P-NDM-7) at room temperature (21°C) and at our optimised hybridisation temperature (40°C). **Figure 4A** shows significantly higher miR-122 target specificity for P-miR-122 at 40°C as compared to room temperature. We further verified the target specificity of P-miR-122 in the flow condition and in the presence of different miRNA targets with various levels of homology such as common isoforms, single nucleotide mismatch,

nearly-complementary and non-complementary targets (see **Table S1** for sequences) at 21°C and 40°C (**Figure 4B**). The miR-39 is a nematode miRNA from *Caenorhabditis elegans* and used as non-specific target, while the miR-3591 is a human miRNA with Rfam (RNA family database) classification of miR-122 precursor (RF00684) and considered as nearly-complementary target. The sensor displayed high signals in presence of miR-122 wild-type sequence, whereas lower signals were obtained with the other targets for both temperatures. The observed cross-reactivity against the highly complementary miR-3591 and miR-122 SNP was further reduced at 40°C. Despite this, the isomiRs, like the wild-type sequence, displayed increased signal at 40°C. The assay detected canonical miR-122 and isomiRs at 40°C. However at 21°C, it only reported the canonical and gave almost the same signal with miR-3591.

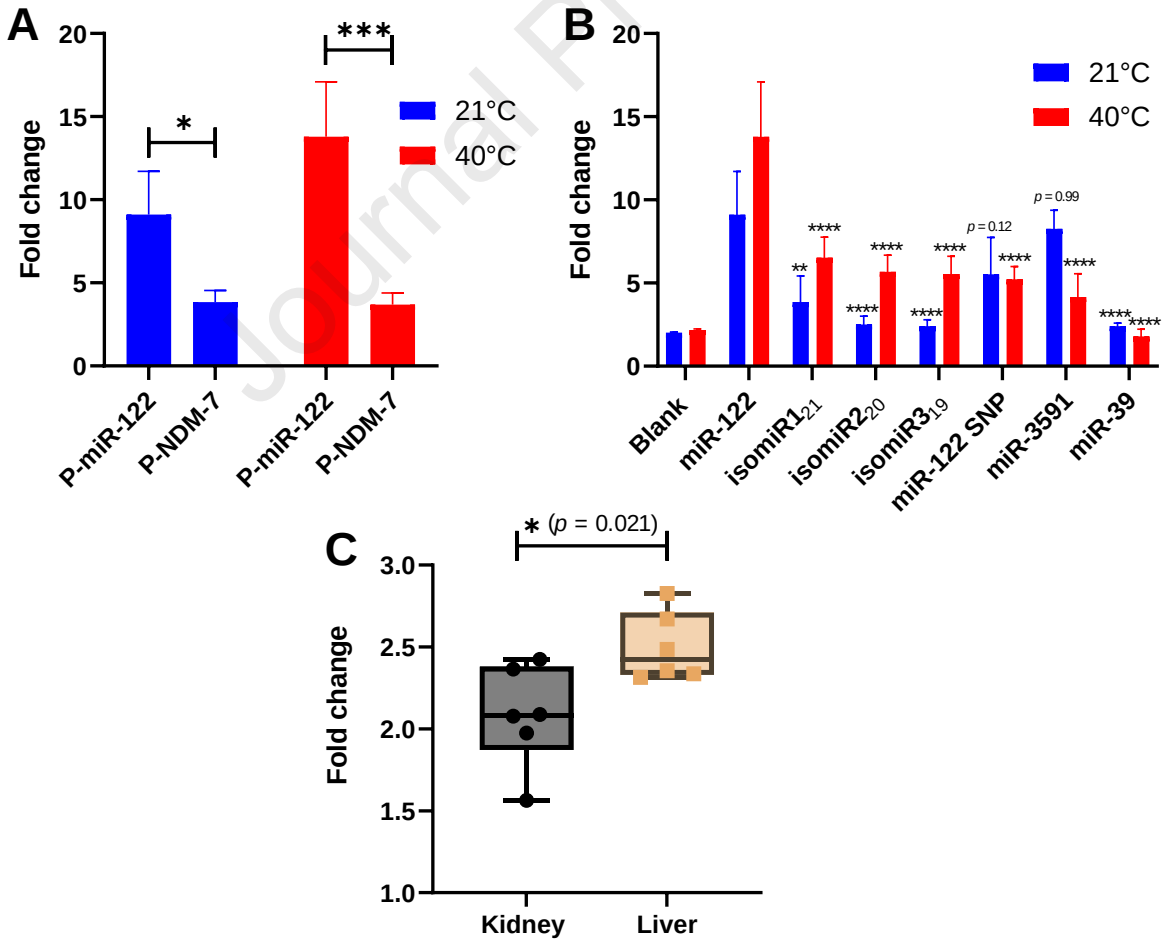

Figure 4 - miR-122 specificity studies in closed-loop flow format. (A) EIS signals (fold change) from electrodes functionalised with 1.5 µM P-miR-122 or P-NDM-7 (control) probes after 60 min incubation with 10 nM of miR-122 target at 21°C or 40°C; (B) EIS signals (fold change) from electrodes functionalised with 1.5 µM P-miR-122 after 60 min incubation with background buffer (blank) or 10 nM each of miR-122 (22 nt), isomiR1 (21 nt), isomiR2 (20 nt), isomiR3 (19 nt), miR-122 SNP (22 nt), miR-3591 (23 nt) and miR-39 (22 nt) targets at 21°C or 40°C; (C) EIS signals (fold change) from electrodes functionalised with 1.5 µM P-miR-122 and after 30 min incubation with mouse kidney (low miR-122) or liver (high miR-122) tissue-extracted samples with 100 times dilution in the background buffer at 40°C. All measurements were conducted in continuous flow with 100 µL/min flow rate. Data in A and B represents the mean ± SD; n = 3. Statistical significance has been determined using a 2-way ANOVA test (significance codes: **** $p \leq 0.0001$, *** $p \leq 0.001$, ** $p \leq 0.01$, * $p \leq 0.05$, compared to miR-122 signals in B). Data in C represents the mean ± SD; n = 6. Statistical significance has been determined using an unpaired t test.

The sensor was further evaluated with mouse tissue-extracted samples at 40°C for confirmation of the sensor specificity for miR-122 in complex biological samples. **Figure 4C** demonstrates a significantly higher signal from the liver samples (high miR-122 expected), as compared to the kidney samples (low miR-122 expected).

3.6. Clinical patient sample analysis

We validated our assay by analysing 26 patient serum samples from the Markers and Paracetamol Poisoning **(**MAPP2) clinical study. The ALT activity of individual serum samples was measured as part of the routine clinical care in Royal Infirmary of Edinburgh (RIE) clinical biochemistry laboratory and used to categorise the samples as liver injury (ALT > 100 U/L) or healthy (ALT < 100 U/L). The serum samples were then analysed using the EIS biosensor in the flow system after standard bench kit microRNA extraction. **Figure 5A** shows significantly higher EIS signal (fold change) in the liver injury samples as compared to the healthy controls. The detection of miR-122 using the EIS was compared with the gold-standard RT-qPCR

measurements, which demonstrated a higher signal for the diseased samples as compared to the healthy controls with significant differences (**Figure 5C)**. The sensitivity and specificity of EIS (**Figure 5B**) and RT-qPCR (**Figure 5D**) measurements were determined from the receiver operator characteristic (ROC) curves, which showed comparable area under the curve (AUC) values (0.77 for EIS and 0.83 for RT-qPCR).

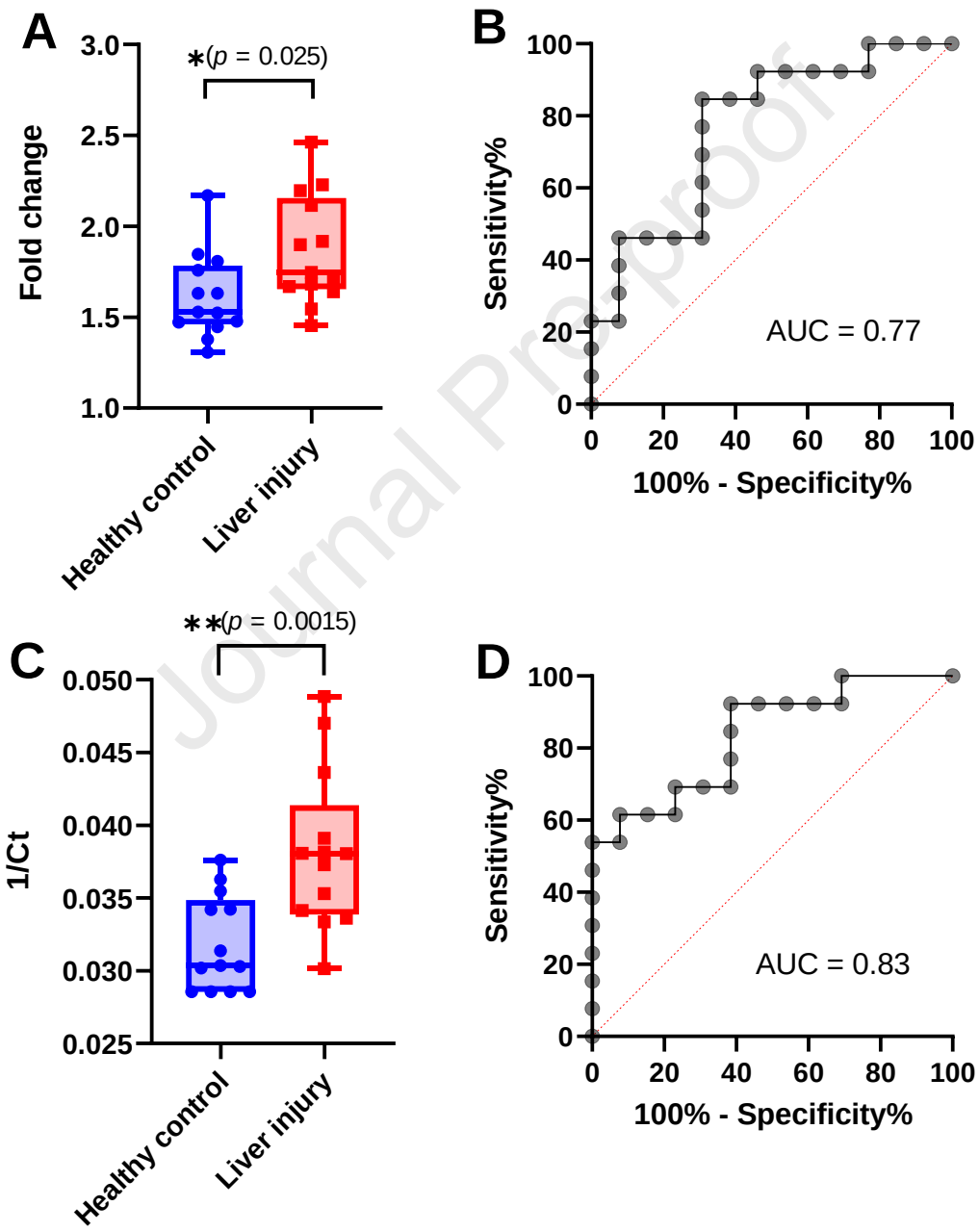

Figure 5 - Patient sample analysis from clinical study. (A) EIS signals (fold change) from electrodes functionalised with 1.5 µM P-miR-122 after 33 min incubation with standard bench-extracted miR-122 in liver injured (n = 13) and healthy control (n = 13) serum samples after 46 times dilution in background buffer. Measurements were conducted in 100 µL/min flow rate and 40°C hybridisation temperature and plotted in the healthy control or liver injury categories, based on ALT activity; (B) receiver operator characteristic (ROC) curve of the EIS results (area under curve, AUC = 0.77 (95% confidence interval (CI): 0.58 - 0.95), sensitivity 0.46 (95% CI: 0.23 - 0.71) at 0.92 specificity); (C) comparison of EIS data with respective qPCR cycle threshold (Ct) values; (D) ROC curve of the qPCR results (area under curve, AUC = 0.83 (95% CI: 0.68 - 0.99), sensitivity 0.62 (95% CI: 0.36 - 0.82) at 0.92 specificity). Data represent the mean ± SD; n = 13. Statistical significance has been determined using an unpaired t test (significance codes: ** $p \leq 0.01$, * $p \leq 0.05$). The AUC value in the ROC curves was determined by using Wilson/Brown test with 95% confidence interval.

4. Discussion

In present study, commercially available screen-printed gold electrodes were functionalised with specific PNA probe molecules to develop a disposable biosensor for miR-122 detection. The bare electrodes have a rough surface morphology, as observed in AFM and SEM studies, which is to be expected given that the surface was formed by screen printing of gold particles suspended in an ink (Butterworth et al. 2019). Following probe immobilisation, the increasing roughness parameters, the deposition of an additional layer with a less porous electrode surface morphology, and the higher presence of carbon as observed from the AFM, SEM and EDX studies each independently support the existence of a PNA probe layer on electrode surface. Earlier AFM studies also noted the rising roughness parameters upon DNA probe immobilisation on electrode surface (Lee et al. 2014). As supported by previous literature, the increase in peak-to-peak potential separation, reduction in peak current amplitudes and a lower surface concentration of ionic species from the CV studies indicate the presence of PNA probes on the electrode interface, which interrupt the reversible redox reaction and the facile electron transfer between electrolyte and electrode (Steel et al. 1998).

The ratio of oxidation and reduction peak current is less than 1 in the probe-modified electrode, confirming the quasi-reversible behaviour of the prepared electrode, which we anticipate resulting from the biological layer of the probe molecules.

During miR-122 target detection using probe-functionalised electrodes, hybridisation under flow-based conditions showed significantly higher EIS signals as compared to static conditions, owing to convective transport of the targets to the surface-immobilised probes and producing faster hybridisation kinetics. As shown in **equation S4** for deducing the Péclet number, convective transport becomes more dominant than molecular diffusion in a flow condition and with increasing flow rates. Accordingly, we hypothesized that as the flow rate increases, the concentration gradient of the target inside the flow cell increases, leading to faster depletion of targets and reduction of diffusion layer thickness on the electrode surface following the hybridisation. However, our experimental data (**Figures 2A** and **S2**) show that the hybridisation signal became stable after 100 µL/min flow rate. This can be attributed by conducting measurements in a closed-loop assembly with a fixed volume of target solution and faster flow rates that give the target molecules less time inside the hybridisation chamber. As a result, target molecules were lacking in sufficient time to diffuse through the self-assembled monolayer (SAM) of PNA probes on the electrode surface. As the electrodes were placed at the bottom of the flow chamber, a large number of target molecules was passing over, instead of diffusing into the SAM layer of the probe molecules. The obtained results suggest that, while taking into account 60 minute end-point data, a flow rate of 100 µL/min was adequate to reach stabilisation of hybridisation kinetics with existing flow cell geometry. In a previous study, Kim and colleagues observed similar pattern on DNA hybridisation kinetics in a flow-based system (Kim et al. 2006). This study showed maximum hybridisation signal at a lower flow rate (1 µL/min versus 4, 7 and 10 µL/min) with 50 pM target concentration, 50 µm channel height, 6 µL sample volume and at a duration of 2 min. Although, as per the finding of this

study and according to the **equation S5**, the hybridisation rate at flow conditions can be enhanced by reducing the flow chamber height. The reduction of total diffusion distance of target molecules to the surface-bound probes on the electrode at the bottom of the flow chamber and the faster convective transport of targets into the flow chamber is suggested to reduce the diffusion layer thickness following the hybridisation and faster hybridisation kinetics. During temperature variation, our EIS measurements nearly followed the temperature profile of a typical surface melting curve, which exhibits a steady high signals below the melting temperature (T_m) of probe-target duplex, followed by a 50% signal reduction at the T_m (Qiao et al. 2015). Our measurements in **Figure 2B** suggest that the temperature of 50°C was close or just above the T_m value, whereas more than half of the targets were dissociated from the probe molecules by the temperature of 60°C. Theoretically, with an oligonucleotide concentration of 50 nM, the basic T_m value of the miR-122 probe/target duplex in solution is 53°C. A previous study showed that the T_m values of surface-bound DNA probes were lowered than the solution-based hybridisation (Ozel et al. 2012). Nevertheless, the calculated basic T_m value strongly correlates our experimental findings.

During dose response studies, we observed a constant increase in EIS signal with the increasing target concentrations due to the availability of more targets for binding at higher concentrations. Although, the kinetics curves (**Figure 3A**) indicate signal saturation for 10 nM or at higher concentrations with a faster saturation with the increasing concentrations. Previous studies on binding kinetics of surface bound PNA/DNA probes with their complementary targets also showed target concentration dependent hybridisation signals with a faster saturation with the increasing concentrations (Jensen et al. 1997; Munir et al. 2017). Our observation suggests that all the available probe binding sites on the electrode surface were saturated with ≥ 10 nM concentrations within 60 min in the closed-loop continuous flow measurements. This results also support our finding in **Figure 2A** where we observed signal

stabilisation at 100 µL/min flow rate with 10 nM target concentration. Beside this, we achieved a limit of detection (LoD) of 50 pM during direct detection of miR-122 using our assay. A previous study on liver injury and miR-122 detection found a mean value of 71.3 million (95% CI 29.3 - 113.2 million) copies/mL of miR-122 in serum for a group of 18 healthy volunteers (McCrae et al. 2016), and the level of miR-122 was elevated 100-10,000 fold in response to drug-induced liver injury (López-Longarela et al. 2020; Starkey Lewis et al. 2011; Vliegenthart et al. 2015a). In healthy serum, 71.3 million copies/mL miR-122 represent 118.5 fM, while in the diseased condition, the concentration can increase to a range of 11.85 pM to 1.185 nM. Additionally, previous work on determining paracetamol toxicity in rat plasma samples showed that the concentration of miR-122 can range between 32 pM and 5.35 nM, when treated with a single dose of paracetamol (1500 mg/kg oral) (López-Longarela et al. 2020). Therefore, the LoD of our assay is within the clinical range and our biosensor detected a higher miR-122 signal in DILI patients. MiR-122 detection in DILI diagnosis has been reported using dynamic chemical labelling (Bowler et al. 2010), combined with bead-based detection using different optical readers such as Simoa SR-X (López-Longarela et al. 2020; Rissin et al. 2017), Luminex MAGPIX fluorescence (Marín-Romero et al. 2020; Venkateswaran et al. 2016) and time-gated fluorescence imaging (Garcia-Fernandez et al. 2019) systems. Some of these studies have achieved more sensitive detection than EIS, but at the expense of methodological complexity. Besides, electrochemical techniques and readers have high utility in terms of simplicity and ease-in-miniaturisation as compared to the fluorescence and other optical methods. Using EIS, we previously explored fundamental parameters influencing sequence-specific miRNA binding by altering the probe length, orientation of probe immobilisation, target overhangs, and degrees of base overhang on the electrode surface (Roychoudhury et al. 2022). Our established model analysis and experiments showed that target overhangs on the electrode surface caused shorter probes to produce stronger EIS signals, and the EIS signal was proportionally higher

with increasing lengths of the overhangs. By using the short probe and target overhangs on the electrode surface, we obtained a LoD of 1 nM for miR-122 at no-flow and room temperature. Although, we further improve the LoD to 50 pM in the present study, with the help of flow measurements and optimised temperature, even after using size-matched probe. **Table S4** compares the analytical performance for miR-122 detection of our EIS assay with other studies, and **Table S5** outlines the advantages and drawbacks of using EIS for miRNA sensing. Nonetheless, our studies demonstrate an EIS-based detection of miR-122 that can provide a LoD within the clinical range while being relatively simple, low-cost and easy-to-implement in the point-of-care setting.

The non-specific binding or adsorption of interferences in real samples can have a strong impact on EIS signals (Bogomolova et al. 2009). We minimised this effect by optimising the reaction temperature, which helped to bind the perfectly-matched target to the probe and not the mismatched interferences. As we can expect lower melting temperatures for interferences and unspecific hybridisations compared to perfectly-matched probe/target complex, specificity can be improved by taking measurements close to the melting temperature of the perfectly-matched probe/target duplex. A sequential washing step would be useful, since it would remove the dissociated interferences and reduce the mismatch signal while maintaining the perfectly-hybridised target signal. While this could help to discriminate the desired target binding from the various interferences during actual sample analysis, this would come at the cost of a more complex system, which is why this was not investigated in this point-of-care application. Although, we observed distinct signals for the P-miR-122 probe (**Figure 4A**) or miR-122 target (**Figure 4B**) among other negative controls at room temperature under non-stringent conditions, the further improvement in specificity at the optimised hybridisation temperature supports our hypothesis. We envisage that measurements conducted at 40°C facilitated in selective detection of miR-122 in liver and kidney tissue-extracted murine

samples. The significant higher signals for liver samples, compared to kidney samples (control) further confirms the specificity of our assay when analysing clinical samples.

Finally, we conducted a feasibility study with patient samples for assay validation and to determine accuracy for DILI diagnostics. The significantly higher signals for the diseased samples as compared to the healthy controls and the comparable sensitivity and specificity with gold-standard qPCR analysis demonstrate the consistent performance of the EIS assay. The AUC of the EIS was close to that of qPCR, which indicates high accuracy of our assay without any amplification of the targets. The diagnostic performance of our EIS assay using such low complexity set-up provides an ideal platform for sample-to-answer system for early diagnosis of DILI at point-of-care.

5. Conclusions

Our study presents the successful development of an assay for detection of unamplified microRNA in a point-of-care compatible format. Electrochemical impedance spectroscopy in combination with disposable, low cost electrodes, peptide nucleic acid probes to provide specificity and a microfluidic setup to enhance hybridisation kinetics enabled specific detection of the miR-122 target biomarker at clinically relevant concentrations. The performance of this biosensor was demonstrated for murine tissue samples as well as human patients with matching performance to qPCR. We therefore will target the full integration of all assay steps in a single sample-to-answer test which can be deployed to any setting where it is needed to detect and manage drug-induced liver injury.

Acknowledgement

The authors acknowledge financial support from the Rosetrees Trust (Ref. no. CF1\100010). We thank Dr. Holger Schulze for useful discussion and the Bioimaging and Cryo FIB-SEM facilities at the University of Edinburgh for the AFM and SEM measurements, respectively.

Author JD acknowledges the support from the Chief Scientist's Office Scotland via the Centre for Precision Cell Therapy for the Liver (PMAS/21/07).

References:

Antoine, D.J., Dear, J.W., Lewis, P.S., Platt, V., Coyle, J., Masson, M., Thanacoody, R.H., Gray, A.J., Webb, D.J., Moggs, J.G., Bateman, D.N., Goldring, C.E., Park, B.K., 2013. Hepatology 58(2), 777-787.

Bernal, W., Williams, R., 2018. Hepatol. Int. 12(3), 204-213.

Björnsson, E.S., Bergmann, O.M., Björnsson, H.K., Kvaran, R.B., Olafsson, S., 2013. Gastroenterology 144(7), 1419-1425.

Björnsson, E.S., Stephens, C., Atallah, E., Robles-Diaz, M., Alvarez-Alvarez, I., Gerbes, A., Weber, S., Stirnimann, G., Kullak-Ublick, G., Cortez-Pinto, H., 2022. A new framework for advancing in drug-induced liver injury research. The Prospective European DILI Registry. Liver international.

Bogomolova, A., Komarova, E., Reber, K., Gerasimov, T., Yavuz, O., Bhatt, S., Aldissi, M., 2009. Anal. Chem. 81(10), 3944-3949.

Bowler, F.R., Diaz-Mochon, J.J., Swift, M.D., Bradley, M., 2010. Angew. Chem. Int. Ed. 49(10), 1809-1812.

Bruch, R., Johnston, M., Kling, A., Mattmüller, T., Baaske, J., Partel, S., Madlener, S., Weber, W., Urban, G.A., Dincer, C., 2021. Biosens. Bioelectron. 177, 112887.

Butterworth, A., Blues, E., Williamson, P., Cardona, M., Gray, L., Corrigan, D.K., 2019. Biosensors 9(1), 22.

De Rie, D., Abugessaisa, I., Alam, T., Arner, E., Arner, P., Ashoor, H., Åström, G., Babina, M., Bertin, N., Burroughs, A.M., Carlisle, A.J., 2017. Nat. Biotechnol. 35(9), 872-878.

Dear, J.W., Antoine, D.J., Starkey-Lewis, P., Goldring, C.E., Park, B.K., 2014. Br. J. Clin. Pharmacol. 77(5), 904-905.

Dear, J.W., Clarke, J.I., Francis, B., Allen, L., Wraight, J., Shen, J., Dargan, P.I., Wood, D., Cooper, J., Thomas, S.H.L., Jorgensen, A.L., Pirmohamed, M., Park, B.K., Antoine, D.J., 2018. Lancet Gastroenterol. Hepatol. 3(2), 104-113.

Edman, C.F., Raymond, D.E., Wu, D.J., Tu, E., Sosnowski, R.G., Butler, W.F., Nerenberg, M., Heller, M.J., 1997. Nucleic Acids Res. 25(24), 4907-4914.

Garcia-Fernandez, E., Gonzalez-Garcia, M.C., Pernagallo, S., Ruedas-Rama, M.J., Fara, M.A., López-Delgado, F.J., Dear, J.W., Ilyine, H., Ress, C., Díaz-Mochón, J.J., Orte, A., 2019. Chem. Comm. 55(99), 14958-14961.

Giacomini, K.M., Krauss, R.M., Roden, D.M., Eichelbaum, M., Hayden, M.R., Nakamura, Y., 2007. Nature 446(7139), 975-977.

Gong, S., Li, J., Pan, W., Li, N., Tang, B., 2021. Anal. Chem. 93(30), 10719-10726.

Huang, X., Li, J., Lu, M., Zhang, W., Xu, Z., Yu, B.-Y., Tian, J., 2020. Anal. Chim. Acta 1112, 72-79.

Jensen, K.K., Ørum, H., Nielsen, P.E., Nordén, B., 1997. Biochemistry 36(16), 5072-5077.

Kaplowitz, N., 2005. Nat. Rev. Drug Discov. 4(6), 489-499.

Kerr, E., Farr, R., Doeven, E.H., Nai, Y.H., Alexander, R., Guijt, R.M., Prieto-Simon, B., Francis, P.S., Dearnley, M., Hayne, D.J., Henderson, L.C., Voelcker, N.H., 2021. Sens. Actuators B Chem. 330, 129261.

Kersaudy-Kerhoas, M., Liga, A., Roychoudhury, A., Stamouli, M., Grant, R., Carrera, D.S., Schulze, H., Mielczarek, W., Oosthuyzen, W., Quintana, J.F., Dickinson, P., Buck, A.H., Leslie, N.R., Haas, J., Bachmann, T.T., Dear, J.W., 2022. Biomicrofluidics 16(2), 024108.

Kia, R., Kelly, L., Sison-Young, R.L., Zhang, F., Pridgeon, C.S., Heslop, J.A., Metcalfe, P., Kitteringham, N.R., Baxter, M., Harrison, S., Hanley, N.A., 2015. Toxicol. Sci. 144(1), 173-185.

Kim, J.H.-S., Marafie, A., Jia, X.-Y., Zoval, J.V., Madou, M.J., 2006. Sens. Actuators B Chem. 113(1), 281-289.

Lee, H.-E., Kang, Y.O., Choi, S.-H., 2014. Int. J. Electrochem. Sci. 9(12), 6793-6808.

Lee, W.M., 2004. Hepatology 40(1), 6-9.

Lee, W.M., 2013. Clin. Liver Dis. 17(4), 575-586.

Lisdat, F., Schäfer, D., 2008. Anal. Bioanal. Chem. 391(5), 1555-1567.

Liu, D., Wang, J., Wu, L., Huang, Y., Zhang, Y., Zhu, M., Wang, Y., Zhu, Z., Yang, C., 2020. Trends Anal. Chem. 122, 115701.

Liu, R.H., Lenigk, R., Druyor-Sanchez, R.L., Yang, J., Grodzinski, P., 2003. Anal. Chem. 75(8), 1911-1917.

López-Longarela, B., Morrison, E.E., Tranter, J.D., Chahman-Vos, L., Léonard, J.-F., Gautier, J.-C., Laurent, S., Lartigau, A., Boitier, E., Sautier, L., Carmona-Saez, P., Martorell-Marugan, J., Mellanby, R.J., Pernagallo, S., Ilyine, H., Rissin, D.M., Duffy, D.C., Dear, J.W., Díaz-Mochón, J.J., 2020. Anal. Chem. 92(4), 3388-3395.

Lu, Z., Wang, H., Naqvi, S.R., Fu, H., Zhao, Y., Song, H., Christen, J.B., 2015. In 2015 28th IEEE International System-on-Chip Conference (SOCC) (pp. 240-244). IEEE.

Lundegard, M., Nylander, K., Danielsson, K., 2015. Med. Oral Patol. Oral Cir. Bucal 20(2), e130.

Marín-Romero, A., Tabraue-Chávez, M., Dear, J.W., Sánchez-Martín, R.M., Ilyine, H., Guardia-Monteagudo, J.J., Fara, M.A., López-Delgado, F.J., Díaz-Mochón, J.J., Pernagallo, S., 2020. Talanta 219, 121265.

McCrae, J.C., Sharkey, N., Webb, D.J., Vliegenthart, A.D.B., Dear, J.W., 2016. Clin. Toxicol. 54(1), 53-55.

McNaught, A.D., Wilkinson, A., 1997. Compendium of chemical terminology. Blackwell Science Oxford.

Munir, A., Waseem, H., Williams, M.R., Stedtfeld, R.D., Gulari, E., Tiedje, J.M., Hashsham, S.A., 2017. Microarrays 6(2), 9.

Ozel, A.B., Srivannavit, O., Rouillard, J.-M., Gulari, E., 2012. Biotechnol. Prog. 28(2), 556-566.

Park, B.K., Dear, J.W., Antoine, D.J., 2015. BMJ clinical evidence, 2015.

Qiao, W., Chiang, H.-C., Xie, H., Levicky, R., 2015. Chem. Comm. 51(97), 17245-17248.

Rahmann, S., Martin, M., Schulte, J.H., Köster, J., Marschall, T., Schramm, A., 2013. Methods 59(1), 154-163.

Rissin, D.M., López-Longarela, B., Pernagallo, S., Ilyine, H., Vliegenthart, A.D.B., Dear, J.W., Díaz-Mochón, J.J., Duffy, D.C., 2017. PloS one 12(7), e0179669.

Ronkainen, N.J., Halsall, H.B., Heineman, W.R., 2010. Chem. Soc. Rev. 39(5), 1747-1763.

Roychoudhury, A., Basu, S., Jha, S.K., 2016. Biosens. Bioelectron. 84, 72-81.

Roychoudhury, A., Dear, J.W., Bachmann, T.T., 2022. Biosens. Bioelectron. 212, 114404.

Roychoudhury, A., Prateek, A., Chauhan, N., Kumar, D.S., Basu, S., Jha, S.K., 2017. ChemistrySelect 2(21), 6118-6128.

Sgro, C., Clinard, F., Ouazir, K., Chanay, H., Allard, C., Guilleminet, C., Lenoir, C., Lemoine, A., Hillon, P., 2002. Hepatology 36(2), 451-455.

Shen, T., Liu, Y., Shang, J., Xie, Q., Li, J., Yan, M., Xu, J., Niu, J., Liu, J., Watkins, P.B., Aithal, G.P., 2019. Gastroenterology 156(8), 2230-2241.

Shi, L., Lei, J., Zhang, B., Li, B., Yang, C.J., Jin, Y., 2018. ACS Appl. Mater. Interfaces 10(15), 12526-12533.

Shin Low, S., Pan, Y., Ji, D., Li, Y., Lu, Y., He, Y., Chen, Q., Liu, Q., 2020. Sens. Actuators B Chem. 308, 127718.

Sosnowski, R.G., Tu, E., Butler, W.F., O'Connell, J.P., Heller, M.J., 1997. Proc. Natl. Acad. Sci. U.S.A. 94(4), 1119-1123.

Starkey Lewis, P.J., Dear, J., Platt, V., Simpson, K.J., Craig, D.G.N., Antoine, D.J., French, N.S., Dhaun, N., Webb, D.J., Costello, E.M., Neoptolemos, J.P., Moggs, J., Goldring, C.E., Park, B.K., 2011. Hepatology 54(5), 1767-1776.

Starkey Lewis, P.J., Merz, M., Couttet, P., Grenet, O., Dear, J., Antoine, D.J., Goldring, C., Park, B.K., Moggs, J.G., 2012. Clin. Pharm. Therap. 92(3), 291-293.

Steel, A.B., Herne, T.M., Tarlov, M.J., 1998. Anal. Chem. 70(22), 4670-4677.

Tavallaie, R., McCarroll, J., Le Grand, M., Ariotti, N., Schuhmann, W., Bakker, E., Tilley, R.D., Hibbert, D.B., Kavallaris, M., Gooding, J.J., 2018. Nat. Nanotechnol. 13(11), 1066-1071.

Turner, A.P.F., 2013. Chem. Soc. Rev. 42(8), 3184-3196.

Válóczi, A., Hornyik, C., Varga, N., Burgyán, J., Kauppinen, S., Havelda, Z., 2004. Nucleic Acids Res. 32(22), e175-e175.

Venkateswaran, S., Luque-González, M.A., Tabraue-Chávez, M., Fara, M.A., López-Longarela, B., Cano-Cortes, V., López-Delgado, F.J., Sánchez-Martín, R.M., Ilyine, H., Bradley, M., Pernagallo, S., Díaz-Mochón, J.J., 2016. Talanta 161, 489-496.

Vliegenthart, A.D.B., Antoine, D.J., Dear, J.W., 2015a. Br. J. Clin. Pharmacol. 80(3), 351-362.

Vliegenthart, A.D.B., Shaffer, J.M., Clarke, J.I., Peeters, L.E.J., Caporali, A., Bateman, D.N., Wood, D.M., Dargan, P.I., Craig, D.G., Moore, J.K., Thompson, A.I., Henderson, N.C., Webb, D.J., Sharkey, J., Antoine, D.J., Park, B.K., Bailey, M.A., Lader, E., Simpson, K.J., Dear, J.W., 2015b. Sci. Rep. 5(1), 15501.

Wang, B., Xi, Y., 2013. Microarrays 2(2), 34-50.

Wang, C., Zhang, Y., Liu, C., Gou, S., Hu, S., Guo, W., 2023. Biosens. Bioelectron. 225, 115073.

Wang, J., 2006. Biosens. Bioelectron. 21(10), 1887-1892.

Wang, K., Zhang, S., Marzolf, B., Troisch, P., Brightman, A., Hu, Z., Hood, L.E., Galas, D.J., 2009. Proc. Natl. Acad. Sci. U.S.A. 106(11), 4402-4407.

Wang, N., Zhang, J., Xiao, B., Sun, X., Xie, R., Chen, A., 2022. Biosens. Bioelectron. 211, 114345.

Wang, X., Chen, X., Ma, X., Kong, X., Xu, Z., Wang, J., 2011. Talanta 84(2), 565-571.

Yang, L., Chen, T., 2017. In 2017 IEEE Biomedical Circuits and Systems Conference (BioCAS) (pp. 1-4). IEEE.

Yu, C.-Y., Yin, B.-C., Ye, B.-C., 2013. Chem. Comm. 49(74), 8247-8249.

Zhou, P., Lu, F., Wang, J., Wang, K., Liu, B., Li, N., Tang, B., 2020. Chem. Comm. 56(63), 8968-8971.

Conflict of interest statement

All authors declare that they have no conflicts of interest.

Declaration of interests

☒ The authors declare that they have no known competing financial interests or personal relationships that could have appeared to influence the work reported in this paper.

☐ The authors declare the following financial interests/personal relationships which may be considered as potential competing interests: